International Journal of Innovative
Computing, Information and Control
Volume 8, Number 9, September 2012

ICIC International ©2012 ISSN 1349-4198
pp. 6081–6093

STATIC OUTPUT FEEDBACK ROBUST LOOP SHAPING CONTROL FOR GRID CONNECTED INVERTER USING GENETIC ALGORITHMS

Natthaphob Nimpitiwan[1] and Somyot Kaitwanidvilai[2,3]

[1]Department of Electrical Engineering
School of Engineering
Bangkok University
Phahonyothin Road, Prathum Thani, Thailand
natthaphob.n@bu.ac.th

[2]Electrical Engineering Department
Faculty of Engineering
[3]Center of Excellence for Innovative Energy Systems
King Mongkut's Institute of Technology Ladkrabang
Chalongkrung Rd. Ladkrabang, Bangkok 10520, Thailand
drsomyotk@gmail.ac.th; kksomyot@kmitl.ac.th

Received June 2011; revised October 2011

Abstract. *At present, robust analysis is an important issue for designing controllers in inverter-based distributed generation systems. In these systems, the fluctuation of DC voltage level from renewable resources (e.g., fuel cells, solar cells, wind turbines) and loading conditions cause system uncertainties and disturbances. To enhance the robust performance of the DG systems, a new class of inverter controller is required to achieve both robustness and performance of entire systems. In this paper, the proposed technique applies Genetic Algorithms (GA) to determine the optimal controller parameters so that stability margin of the controlled system is maximized. In addition, the structure of (Proportional-Integral-Derivative) PID with first order derivation filter is selected as the final controller to realize a practical robust controller. As results indicated, stability margin of the proposed controller is better than that of the reduced order controller designed by Hankel Norm model reduction. The proposed technique, hence, offers a robust controller with a guaranteed stability margin; also it is practically feasible to be implemented.*

Keywords: Static output feedback controller, Genetic algorithms, Inverter-based grid connected system

1. **Introduction.** Installed capacity of grid-connected distributed generations (DGs) from renewable sources (e.g., solar cells, fuel cells and wind energy) is significantly increased with fast development of technology to improve efficiency and reliability. Environmental friendly aspects (i.e., zero/fewer waste, water and air pollutions and lesser disrupted land) are main advantages of installing renewable DGs to grid systems. However, especially with high penetration level of renewable DGs, several concerns have to be carefully considered, such as impacts on power system quality, islanded operation, coordination of protection systems, reliability and stability of systems.

Pulse width modulation (PWM) inverters are mainly applied to govern the transformation of energy from renewable DC sources and synchronize DGs to AC grid systems. Several control structures are applied to regulate the operation of inverters, such as Proportional-Integral (PI) controller, Proportional Resonant (PR) controller and Hysteresis controller [1]. Switching model simulations of inverters (e.g., PSpice, Matlab/Simulink

and PSCAD/EMTP) can be performed to verify the desired transient/steady state performance and to assess the impact of installing DGs. By applying switching model simulation, detail analysis in time domain of grid connected inverters with high accuracy can be obtained [2-4]; however, this type of simulation may not be suitable for analyzing large scaled power systems with several inverter-based DGs. For controller design purposes, dynamic operation of inverters can be represented by a linearized state space approach. Steady state model of inverters and further analyses (i.e., modal and eigen analysis, sensitivity analysis) are well studied and can be found in [5-8].

At present, many advanced control techniques (e.g., robust control, adaptive control, intelligent control) are applied to improve the performance of electrical power systems. Robust control has gained more attention due to its high performance and robustness; however, the implementation of the robust controller is still difficult because of the complexity of the resulting controller. In addition, the order of controller designed by this approach is usually higher than the order of typical plants, making it difficult to be implemented in practice. Although there are several powerful model reduction techniques for reducing the order of the robust controller, the stability margin of a system controlled by the reduced order controller is significantly decreased in many cases.

One of the most popular techniques in robust control is H_∞ optimal control. In this technique, two appropriate weights for both uncertainty of model and performance are essentially chosen. A difficulty with the H_∞ optimal control approach is that the appropriate selection of closed-loop objectives and weights is not straightforward [9]. Moreover, especially in a multiple-input and multiple-output (MIMO) system, it is not easy to specify the uncertainty weight in practice. Recently, H_∞ loop shaping control [2] has gained more attention due to its simple design procedure. The uncertainty model in this approach does not represent actual physical uncertainty, which is difficult to be identified in MIMO system. Moreover, the H_∞ loop shaping control is based on the concept of loop shaping technique, which is a well-known technique in classical control. However, the controller designed by H_∞ loop shaping is still complicated. To overcome this problem, several approaches [10-12] have been proposed to design a fixed-structure robust controller. Patra et al. [12] proposed the static output feedback H_∞ loop shaping using Linear Matrix Inequality (LMI) technique. In their design, the structure of resulting controller is the same as the structure of performance weight. In [11], the similar technique was applied to design the power system damping controllers. However, as reported by Somyot [10], LMI approach has a local minima problem which sometimes causes an insufficient stability margin. To improve the stability margin, this paper focuses on the design of the static output feedback controller for grid connected inverter systems. The proposed technique is based on the concept of static output feedback control. Therefore, the structure of the proposed controller is the same as the structure of performance weight which is usually chosen as PI or PID. The stability margin, which is an indicator of robust performance in the proposed technique, is determined by solving the infinity norm of the robust loop shaping technique proposed by McFarlane and Glover [9]. With considering system uncertainties and system performance, design conditions are expressed by applying linear matrix inequalities (LMIs). In [13], R. Vilanova and P. Balagu propose a technique for analyzing interactions among decentralized PI/PID controllers in MIMO systems. The proposed technique is applied to ensure effectiveness and system stability of MIMO systems with decentralized controllers.

For renewable energies, several system parameters of inverters (e.g., variations of DC voltage level from renewable resources, voltage drops at the terminal of inverters, variations of coupling impedance) may fluctuate and lead to unexpected operations or loss of system stability. This paper proposes a fixed-structure H_∞ loop shaping controller

design procedure for constant power factor grid-connected inverters. With the proposed design procedure, the robustness of inverter systems (i.e., system stability margin) can be determined with a desired performance. The proposed fixed-structure design offers a major benefit in controller implementation. That is, instead of high-order controller from conventional H_∞ design, a simple low-order controller with desired performance and stability margin is achieved. Moreover, the proposed technique is adopted to design a robust decentralized controller, which gains an advantage of simple structure. In several cases of power systems, centralized controller is not applicable.

The remainder of this paper is organized as follows. Section 2 describes the grid connected inverter system modeling. Section 3 illustrates the proposed technique. Simulations and results are shown in Section 4, and Section 5 concludes the paper.

2. **Grid Connected Inverter System Modeling.** In this paper, the configuration of a grid connected three-phase inverter is shown in Figure 1. Assuming that the inverter is connected to a well regulated voltage and frequency grid system, the inverter is modeled as a constant power factor control mode. DC voltage source (V_S) is provided to the inverter from several possible energy resources (e.g., solar cells, fuel cells). In this paper, the three-phase inverter generates a sinusoidal output voltage by using the carrier-based pulse-width modulation (PWM) technique with the central-aligned triangular waveform. Status of a switching component (i.e., on or off) in each period can be expressed as

$$d_i^* = \begin{cases} 1, & \text{if } (1-d_i)\pi \le \omega_s t \le (1+d_i)\pi \\ 0, & \text{otherwise} \end{cases} \tag{1}$$

where d_i is duty ratio of at each period and ω_s is the switching frequency.

From switching status in (1), the general model of a three-phase inverter can be represented as a time-varying state space model as

$$\dot{x} = Ax + Bu \tag{2}$$

where

$$x = \begin{bmatrix} i_a & i_b & i_c & i_s & v_d & v_{cfa} & v_{cfb} & v_{cfc} & i_A & i_B & i_C \end{bmatrix}'$$
$$u = \begin{bmatrix} e_a & e_b & e_c & v_s \end{bmatrix}'$$

$$A = \begin{bmatrix} -R/L & 0 & 0 & 0 & \frac{1}{L}\left(d_1^* - \frac{1}{3}\sum_{i=1}^{3} d_i^*\right) & -\frac{1}{L} & 0 & 0 & 0 & 0 & 0 \\ 0 & -R/L & 0 & 0 & \frac{1}{L}\left(d_2^* - \frac{1}{3}\sum_{i=1}^{3} d_i^*\right) & 0 & -\frac{1}{L} & 0 & 0 & 0 & 0 \\ 0 & 0 & -R/L & 0 & \frac{1}{L}\left(d_3^* - \frac{1}{3}\sum_{i=1}^{3} d_i^*\right) & 0 & 0 & -\frac{1}{L} & 0 & 0 & 0 \\ 0 & 0 & 0 & -\frac{R_s}{L_s} & -\frac{1}{L_s} & 0 & 0 & 0 & 0 & 0 & 0 \\ \frac{-d_1^*}{C_s} & \frac{-d_2^*}{C_s} & \frac{-d_3^*}{C_s} & \frac{1}{C_s} & 0 & 0 & 0 & 0 & 0 & 0 & 0 \\ \frac{1}{C} & 0 & 0 & 0 & 0 & 0 & 0 & 0 & -\frac{1}{C} & 0 & 0 \\ 0 & \frac{1}{C} & 0 & 0 & 0 & 0 & 0 & 0 & 0 & -\frac{1}{C} & 0 \\ 0 & 0 & \frac{1}{C} & 0 & 0 & 0 & 0 & 0 & 0 & 0 & -\frac{1}{C} \\ 0 & 0 & 0 & 0 & 0 & \frac{1}{L_{line}} & 0 & 0 & -\frac{R_{Line}}{L_{line}} & 0 & 0 \\ 0 & 0 & 0 & 0 & 0 & 0 & \frac{1}{L_{line}} & 0 & 0 & -\frac{R_{Line}}{L_{line}} & 0 \\ 0 & 0 & 0 & 0 & 0 & 0 & 0 & \frac{1}{L_{line}} & 0 & 0 & -\frac{R_{Line}}{L_{line}} \end{bmatrix}$$

$$B = \begin{bmatrix} 0 & 0 & 0 & 0 \\ 0 & 0 & 0 & 0 \\ 0 & 0 & 0 & 0 \\ 0 & 0 & 0 & \frac{1}{L_s} \\ 0 & 0 & 0 & 0 \\ 0 & 0 & 0 & 0 \\ 0 & 0 & 0 & 0 \\ 0 & 0 & 0 & 0 \\ -\frac{1}{L_{line}} & 0 & 0 & 0 \\ 0 & -\frac{1}{L_{line}} & 0 & 0 \\ 0 & 0 & -\frac{1}{L_{line}} & 0 \end{bmatrix}$$

As defined in (1), status of switching components is discrete functions; hence, solving dynamic responses of the inverter is quite complicated. By applying Fourier analysis, the status of switching components can be written as

$$\begin{aligned} d_i^* &= d_i + \sum_{n=1}^{\infty} (-1)^n \cdot \tfrac{2}{n\pi} \sin(n d_i \pi) \cos(n\omega_s \pi) \\ \sum_{i=1}^{3} d_i^* &= \sum_{i=1}^{3} d_i + \sum_{n=1}^{\infty} \left[\sum_{i=1}^{3} (-1)^n \tfrac{2}{n\pi} \sin(n d_i \pi) \right] \cos(n\omega_s \pi) \end{aligned} \tag{3}$$

Substituting (3) in (2), the three-phase inverter model is separated into two major parts: a low-frequency model for power frequency and stability analysis and a high-frequency

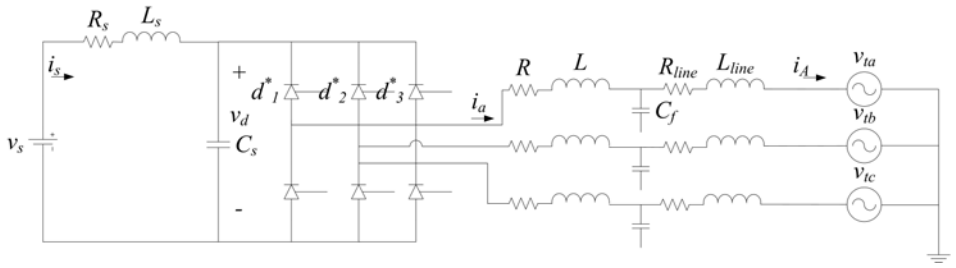

FIGURE 1. Configuration of a three-phase grid connected inverter

model for harmonic analysis. Both models provide continuous governing differential functions of the three phase inverter.

Note that the switching frequency ω_s is much higher than the power frequency. This paper focuses on designing a current controller for the three-phase inverter; therefore, the low-frequency model is employed as a general state space model of the inverter. The dynamic responses at high frequency ($> \omega_s$) are not considered in this paper and expected to be attenuated by LC low-pass filter. Details of the switching components representation for a PWM scheme by applying Fourier analysis are well studied in [6]. For generating controllable output powers (i.e., real power and reactive power) at power frequency ω, the duty ratio d_i for phase i can be expressed in term of phase shift ϕ and modulation index m as

$$d_i = \frac{m}{2}\sin\left[\omega t - (i-1)\frac{2\pi}{3} - \phi\right] + \frac{1}{2} \tag{4}$$

After substituting (3) into (2), the state space representation of the system becomes a continuous time-varying system. To avoid the complication in solving the time-varying system, a transformation is applied using "the rotational frame of reference" [14]. The state and control variables in the stationary frame of reference are transformed to rotational frame of reference by

$$\begin{aligned} x &= Tx_r \\ u &= Pu_r \end{aligned} \tag{5}$$

where

$$T = \frac{1}{\sqrt{3}}\begin{bmatrix}
\frac{1}{\sqrt{2}} & \cos\omega t & \sin\omega t & 0 & 0 & 0 & 0 & 0 & 0 & 0 & 0 \\
\frac{1}{\sqrt{2}} & \cos\left(\omega t - \frac{2\pi}{3}\right) & \sin\left(\omega t - \frac{2\pi}{3}\right) & 0 & 0 & 0 & 0 & 0 & 0 & 0 & 0 \\
\frac{1}{\sqrt{2}} & \cos\left(\omega t + \frac{2\pi}{3}\right) & \sin\left(\omega t + \frac{2\pi}{3}\right) & 0 & 0 & 0 & 0 & 0 & 0 & 0 & 0 \\
0 & 0 & 0 & \frac{3}{\sqrt{2}} & 0 & 0 & 0 & 0 & 0 & 0 & 0 \\
0 & 0 & 0 & 0 & \frac{3}{\sqrt{2}} & 0 & 0 & 0 & 0 & 0 & 0 \\
0 & 0 & 0 & 0 & 0 & \frac{1}{\sqrt{2}} & \cos\omega t & \sin\omega t & 0 & 0 & 0 \\
0 & 0 & 0 & 0 & 0 & \frac{1}{\sqrt{2}} & \cos\left(\omega t - \frac{2\pi}{3}\right) & \sin\left(\omega t - \frac{2\pi}{3}\right) & 0 & 0 & 0 \\
0 & 0 & 0 & 0 & 0 & \frac{1}{\sqrt{2}} & \cos\left(\omega t + \frac{2\pi}{3}\right) & \sin\left(\omega t + \frac{2\pi}{3}\right) & 0 & 0 & 0 \\
0 & 0 & 0 & 0 & 0 & 0 & 0 & 0 & \frac{1}{\sqrt{2}} & \cos\omega t & \sin\omega t \\
0 & 0 & 0 & 0 & 0 & 0 & 0 & 0 & \frac{1}{\sqrt{2}} & \cos\left(\omega t - \frac{2\pi}{3}\right) & \sin\left(\omega t - \frac{2\pi}{3}\right) \\
0 & 0 & 0 & 0 & 0 & 0 & 0 & 0 & \frac{1}{\sqrt{2}} & \cos\left(\omega t + \frac{2\pi}{3}\right) & \sin\left(\omega t + \frac{2\pi}{3}\right)
\end{bmatrix}$$

$$P = \sqrt{2/3}\begin{bmatrix}
1/\sqrt{2} & \cos\omega t & \sin\omega t & 0 \\
1/\sqrt{2} & \cos\left(\omega t - \frac{2\pi}{3}\right) & \sin\left(\omega t - \frac{2\pi}{3}\right) & 0 \\
1/\sqrt{2} & \cos\left(\omega t + \frac{2\pi}{3}\right) & \sin\left(\omega t + \frac{2\pi}{3}\right) & 0 \\
0 & 0 & 0 & \sqrt{3/2}
\end{bmatrix}$$

Assuming that the three-phase inverter is connected to a balanced voltage system with amplitude e_m, (2) can be written in the rotational frame of reference as

$$\dot{x}_r = T^{-1}ATx_r - T^{-1}\dot{T}x_r + T^{-1}BPu_r \tag{6}$$

or

$$\dot{x}_r = A_r x_r + M(x_r, u_r)$$

where

$$x_r = \begin{bmatrix} i_d & i_q & i_s & v_d & v_{cfd} & v_{cfq} & i_D & i_Q \end{bmatrix}'$$

$$A_r = \begin{bmatrix} \frac{-R}{L} & -\omega & 0 & 0 & -\frac{1}{L} & 0 & 0 & 0 \\ \omega & \frac{-R}{L} & 0 & 0 & 0 & -\frac{1}{L} & 0 & 0 \\ 0 & 0 & \frac{-R_s}{L_s} & \frac{-1}{L_s} & 0 & 0 & 0 & 0 \\ 0 & 0 & \frac{1}{C_s} & 0 & 0 & 0 & 0 & 0 \\ \frac{1}{C} & 0 & 0 & 0 & 0 & -\omega & \frac{-1}{C} & 0 \\ 0 & \frac{1}{C} & 0 & 0 & \omega & 0 & 0 & \frac{-1}{C} \\ 0 & 0 & 0 & 0 & \frac{1}{L_{line}} & 0 & \frac{-R_{Line}}{L_{line}} & -\omega \\ 0 & 0 & 0 & 0 & 0 & \frac{1}{L_{line}} & \omega & \frac{-R_{Line}}{L_{line}} \end{bmatrix} \quad M(x_r, u_r) = \begin{bmatrix} \frac{\sqrt{6}}{4L}V_d m_d \\ \frac{\sqrt{6}}{4L}V_d m_q \\ \frac{-1}{L_s}v_s \\ -\frac{\sqrt{6}}{4C_s}I_d m_d + \frac{\sqrt{6}}{4C_s}I_q m_q \\ 0 \\ 0 \\ -\frac{1}{L_{line}}\frac{\sqrt{6}}{2}e_m \cos\varphi \\ +\frac{1}{L_{line}}\frac{\sqrt{6}}{2}e_m \sin\varphi \end{bmatrix}$$

$m_d = m\cos\phi$ and $m_q = m\sin\phi$.

Note from (6) that, by assuming a balanced voltage system, the variables in zero sequence are neglected. The state space equations representing the three-phase inverter in (6) are non-linear functions. Hence, the state space model is linearized and rearranged by expanding (6) into a Taylor series about a nominal operating point; system equations can be written as

$$\begin{bmatrix} \Delta\dot{i}_d \\ \Delta\dot{i}_q \\ \Delta\dot{i}_s \\ \Delta\dot{v}_d \\ \Delta\dot{v}_{cfd} \\ \Delta\dot{v}_{cfq} \\ \Delta\dot{i}_D \\ \Delta\dot{i}_Q \end{bmatrix} = \begin{bmatrix} \frac{-R}{L} & -\omega & 0 & \frac{\sqrt{6}}{4L}m_d & \frac{-1}{L} & 0 & 0 & 0 \\ \omega & \frac{-R}{L} & 0 & \frac{\sqrt{6}}{4L}m_q & 0 & \frac{-1}{L} & 0 & 0 \\ 0 & 0 & \frac{-R_s}{L_s} & \frac{-1}{L_s} & 0 & 0 & 0 & 0 \\ \frac{-\sqrt{6}}{4C_s}m_d & \frac{-\sqrt{6}}{4C_s}m_q & \frac{1}{C_s} & 0 & 0 & 0 & 0 & 0 \\ \frac{1}{C} & 0 & 0 & 0 & 0 & -\omega & \frac{-1}{C} & 0 \\ 0 & \frac{1}{C} & 0 & 0 & \omega & 0 & 0 & \frac{-1}{C} \\ 0 & 0 & 0 & 0 & \frac{1}{L_{line}} & 0 & \frac{-R_{line}}{L_{line}} & -\omega \\ 0 & 0 & 0 & 0 & 0 & \frac{1}{L_{line}} & \omega & \frac{-R_{line}}{L_{line}} \end{bmatrix} \begin{bmatrix} \Delta i_d \\ \Delta i_q \\ \Delta i_s \\ \Delta v_d \\ \Delta v_{cfd} \\ \Delta v_{cfq} \\ \Delta i_D \\ \Delta i_Q \end{bmatrix} + \begin{bmatrix} \frac{\sqrt{6}}{4L}V_d & 0 \\ 0 & \frac{\sqrt{6}}{4L}V_d \\ 0 & 0 \\ -\frac{\sqrt{6}}{4C_s}I_d & \frac{\sqrt{6}}{4C_s}I_q \\ 0 & 0 \\ 0 & 0 \\ 0 & 0 \\ 0 & 0 \end{bmatrix} \begin{bmatrix} \Delta m_d \\ \Delta m_q \end{bmatrix} \tag{7}$$

The modulation indices (m_d and m_q) are considered as control variables in rotational frame of reference. To control the output power of the three-phase inverter (P_{ref} and Q_{ref}), the reference injected currents in d and q axis are determined by

$$i_Q^{ref} = \frac{v_{tq}P^{ref} + v_{td}Q^{ref}}{v_{td}^2 + v_{tq}^2} \quad \text{and} \quad i_Q^{ref} = \frac{v_{tq}P^{ref} + v_{td}Q^{ref}}{v_{td}^2 + v_{tq}^2} \tag{8}$$

Model of the three-phase inverter in a constant power factor control mode is shown in Figure 2. The linearized state space representation of the three-phase inverter in (7) and the power controller in (8) are employed to design the proposed controller.

3. **Static Output Feedback Robust Loop Shaping Control Using Genetic Algorithm.** The proposed technique is based on the concept of static output feedback robust loop shaping control proposed by Patra in [12]. In this technique, the desired open loop singular values of the plant (G) in frequency domain or $\sigma(G)$ is specified by shaping the open loop singular values. Shaping the singular values of plant G is accomplished by applying the weighting functions – pre-compensator (W_1) and post-compensator (W_2). Thus,

$$G_s = W_2 G W_1 \tag{9}$$

The uncertainty model of the system is formulated as normalized co-prime factors that divide the shaped plant (G_s) into nominator factor (N_s) and denominator factor (M_s).

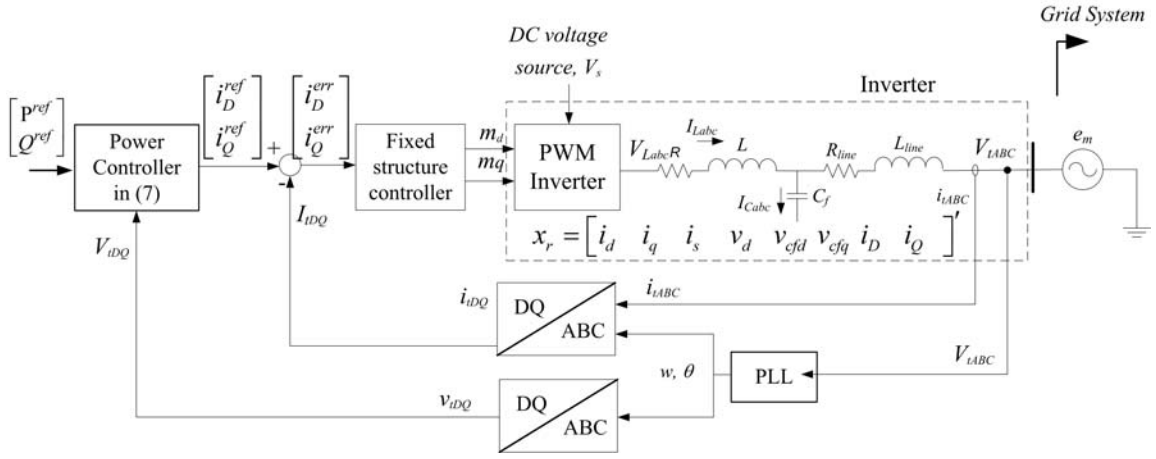

FIGURE 2. Model of the three-phase inverter with the proposed fixed structured controller

In static output feedback robust loop shaping control, the structure of final controller is the same as the structure of the performance weight.

$$K = K_{ST} W_1 \tag{10}$$

where K_{ST} is the constant matrix; K is the final controller and the post compensator W_2 is chosen as identity matrix. In the proposed technique, the matrices of weight and static gain are specified as:

$$W_1 = \begin{bmatrix} k_1 + \frac{k_2}{s} + \frac{k_3 s}{\tau s+1} & 0 \\ 0 & k_4 + \frac{k_5}{s} + \frac{k_6 s}{\tau s+1} \end{bmatrix} \tag{11}$$

and

$$K_{ST} = \begin{bmatrix} k_7 & k_8 \\ k_9 & k_{10} \end{bmatrix} \tag{12}$$

where k_1 to k_{10} are the gain values attempted to be evaluated. Based on the concepts of robust loop shaping and the static output feedback, the optimization problem of the proposed technique can be written as:

Maximize

$$\varepsilon = \|T_{zw}\|_\infty^{-1} = \left\| \begin{bmatrix} I \\ K_{ST}(k_7 \ldots k_{10}) \end{bmatrix} (I + GW_1(k_1 \ldots k_6) K_{ST}(k_7 \ldots k_{10}))^{-1} M_s^{-1} \right\|_\infty^{-1} \tag{13}$$

Subject to

$$\begin{gathered} Lk_1 < k_1 < Uk_1 \\ Lk_2 < k_2 < Uk_2 \\ \vdots \\ Lk_{10} < k_{10} < Uk_{10} \end{gathered}$$

$$\left.\begin{array}{r} \text{Crossover frequency} > \text{CF} \\ (G_S(\omega < \omega_{low\,freq})) \ > LG \\ \overline{\sigma}(G_S(\omega > \omega_{high\,freq})) \ < HG \end{array}\right\} \quad \text{(Constrains in frequency domain)}$$

where CF is the crossover frequency of the desired loop shape of the shaped plant, LG is the specified gain, $(G_S(\omega < \omega_{low\,freq}))$ is the lower singular values shape in low frequency range $(\omega < \omega_{low\,freq})$ of the desired loop shape, HG is the specified gain, $\overline{\sigma}(G_S(\omega > \omega_{high\,freq}))$ is the upper singular values shape in high frequency range $(\omega > \omega_{high\,freq})$ of the desired loop shape. Figure 3 shows the typical loop shape. Lki and Uki are the

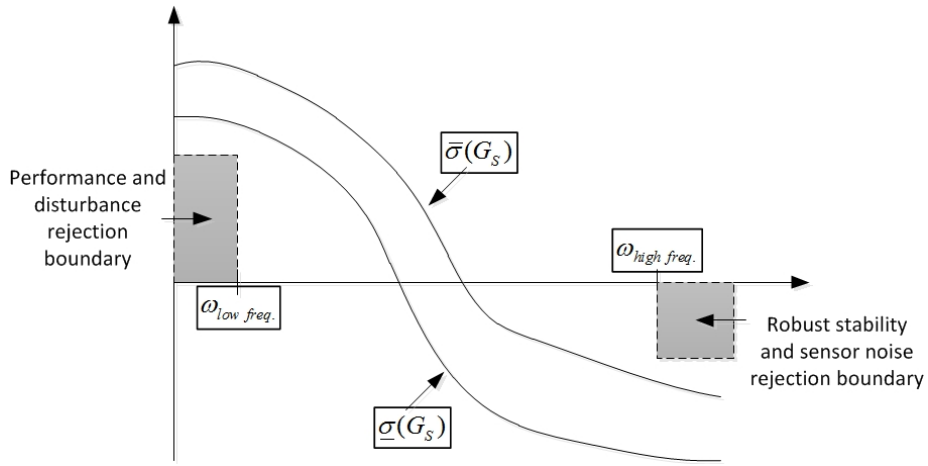

FIGURE 3. Open loop singular value shaping

lower and upper bound values of the parameter k_i, respectively. In this paper, $k1$ to $k10$ are determined by applying the Genetic Algorithm (GA). τ is the time constant which is selected as 0.001 in this paper.

GA is a well-known algorithm that can be applied to many kinds of optimization problems. This algorithm applies concepts of chromosomes and genetic operators to find the generations until the stopping criteria are met. Fitness function is adopted as the indicator of the goodness of a solution which can be written as:

$$f_s = \begin{cases} \varepsilon & \text{if all comply with all constraints} \\ 0.0001 & \text{otherwise} \end{cases} \tag{14}$$

Based on the above mentioned illustrations, the proposed technique can be described as follows.

1. Specify the GA parameters, such as population size, lower and upper bound parameters, probabilities of cross over, mutation and reproduction operations, and method of selection.
2. Randomly initialize the 1st generation.
3. Evaluate the fitness function (f_s) of each chromosome; keep the best chromosome as the solution of the generation.
4. Increment the generation for a step. If the current generation is the maximum generation, then stop. Otherwise, generate the new chromosomes by genetic operators and then go to Step 3.

4. **Simulations and Results.** Robustness properties of the proposed controllers (e.g., robust stability and robust performance) are investigated by performing time domain simulations of a three-phase inverter system as shown in Figure 1. Simulations of the detailed switched model with the proposed controller are accomplished in Matlab/Simulink. At the AC terminal, the three-phase inverter is connected to a grid system with a normal voltage at 380 V. An ideal DC voltage source with rated voltage at 1,900 V is applied as an energy resource. Although, the detail analysis of DC source (e.g., fuel cells, solar cells) can be further accomplished by applying characteristic equations; to reduce the complication in the controller design process, dynamics of the DC voltage source (i.e., solar cells, fuel cells) are not considered in the model. Voltage variations of the DC source vs, considered as a parametric uncertainty, are introduced in simulations to verify the robustness of the proposed controller. By applying the detailed switched model simulations, parameters

of the three-phase inverter grid connected system with a proposed constant power factor controller are shown in Table 1.

TABLE 1. Parameters of a grid connected three phase inverter [15]

Controller parameters	Value
Switching frequency, f	7 kHz
DC voltage source (V_d)	1,900 V_{rated} Varies from 1,425 V to 1,900 V
Rated output voltage (V_T)	380 Vrms, $f = 50$ Hz
Nominal output power (P_L)	500 kW
Grid connection	$R_{Line} = 300$ mΩ, $L_{Line} = 300$ μH, $C_f = 750$ μF
AC-DC inverter	$R_s = 3$ mΩ, $L_s = 3$ μH, $C_s = 5{,}000$ μF

Performance of the proposed controllers are compared with full order controllers and demonstrated in 4 cases as
Case 1: A centralized fixed structure robust loop shaping controller.
Case 2: A centralized full order H_∞ loop shaping (the same performance weight as Case 1).
Case 3: A decentralized fixed structure robust loop shaping controller.
Case 4: A centralized full order H_∞ loop shaping (the same performance weight as Case 3).

The matrix of weight W_1 in (11) is specified as a diagonal matrix to get a desirable singular value of the open-loop transfer function G_s. To achieve an acceptable disturbance rejection, the upper bound singular value of G_s at high frequency (>4,000 rad/s) is reduced to lower than –15 dB. Also, to minimize the steady state error, the lower bound singular value of G_s is raised higher than 10 dB at 50 rad/s. Singular value plots of G and G_s in (9) are shown in Figure 4.

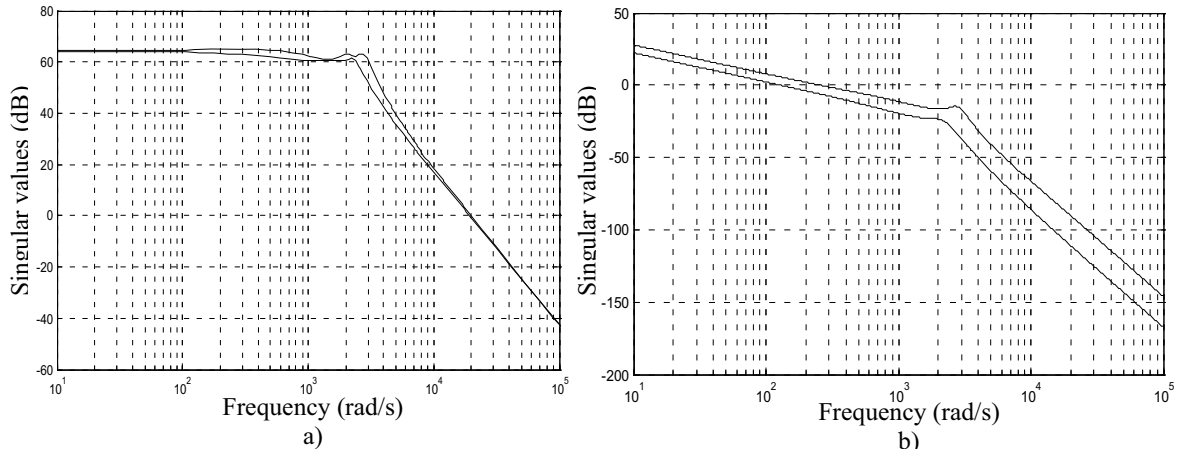

FIGURE 4. Singular values of a) original plant G and b) shaped plant G_s

In Case 1, the proposed controller is designed as a centralized fixed structure PID robust loop shaping controller with order 4. As defined in (9) to (14), the GA is performed to determine parameters of the controller $k1$ to $k10$. The calculation progress of the GA is shown in Figure 5. By minimizing the fitness value in (10), the proposed controller (Case 1) with stability margin 0.584 is derived after 60 iterations.

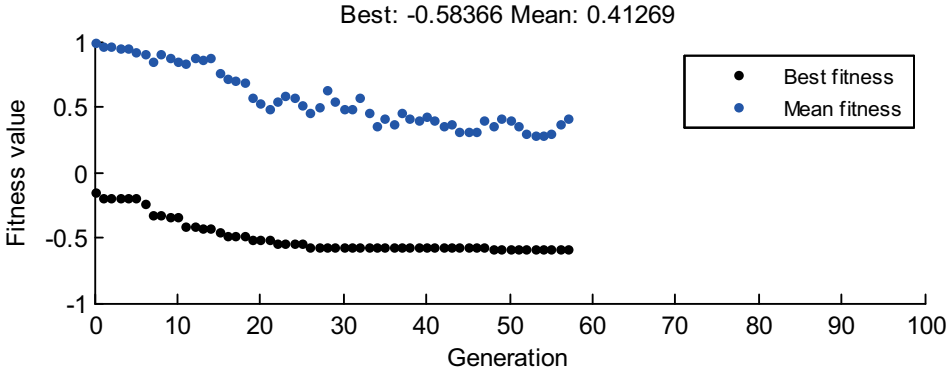

FIGURE 5. Convergence of GA algorithm in Case 1

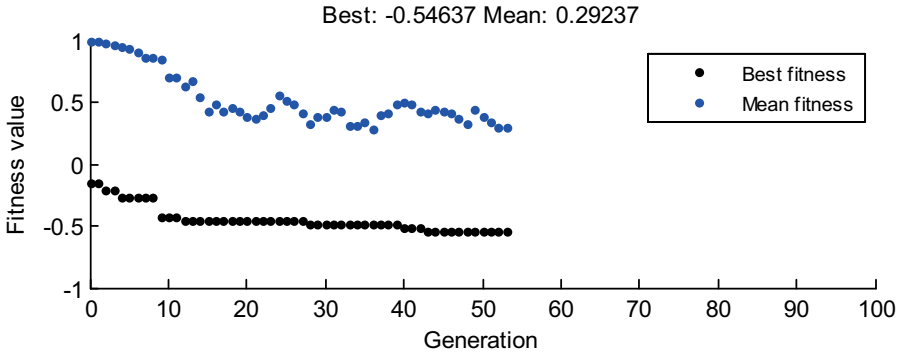

FIGURE 6. Convergence of GA algorithm in Case 3

In Case 2, the centralized full order H_∞ loop shaping controller is synthesized. The performance weight adopted in the design is the same as that of Case 1. The centralized full order controller has order 16 with stability margin 0.615.

In Case 3, the proposed controller is designed as a decentralized fixed structure PID robust loop shaping controller. The structure of the controller is designed with $W1$ as shown in (11) and

$$K_{ST} = \begin{bmatrix} k_7 & 0 \\ 0 & k_8 \end{bmatrix}.$$

In this case, the GA is performed to determine parameters of the controller $k1$ to $k8$ with order 4. After 60 iterations, the proposed controller is derived with stability margin 0.546. The resulting centralized and decentralized controllers designed by the proposed technique are shown in Appendix A.

In Case 4, the centralized full order H_∞ loop shaping controller is synthesized. The performance weight adopted in the design is the same as that of Case 3. With full order controller, the decentralized controller in Case 4 has order 16 with stability margin 0.627.

For comparing performance of the controllers, the proposed fixed structure robust loop shaping controllers in Cases 1 and 3 are compared with the centralized full order H_∞ loop shaping controllers of its own weighting functions in Cases 2 and 4, respectively. Note that, with lesser complicated structure, the stability margin of the decentralized controller in Case 3 has a lower stability margin. However, with the proposed fixed structure controller in Cases 1 and 3, the practical implementations are significantly more convenient.

The proposed three-phase inverter is designed as a unity power factor mode with reference real power output $P_{ref} = 500$ kW. The non-linear state equations in (7) are linearized

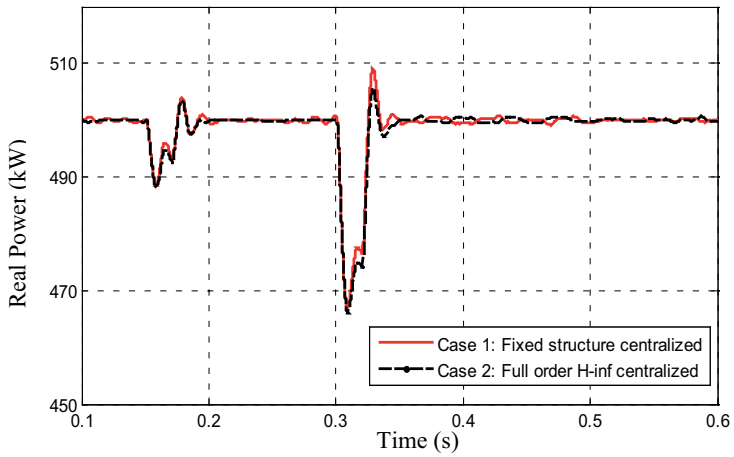

FIGURE 7. DC source voltage change with centralized controllers (Case 1: Proposed fixed structure centralized controller, Case 2: Full order H_∞ centralized controller)

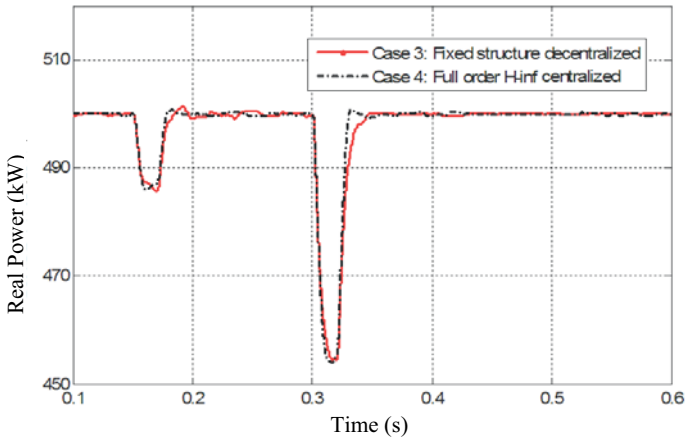

FIGURE 8. DC source voltage change with decentralized controllers (Case 3: Proposed fixed structure decentralized controller, Case 4: Full order H_∞ centralized controller)

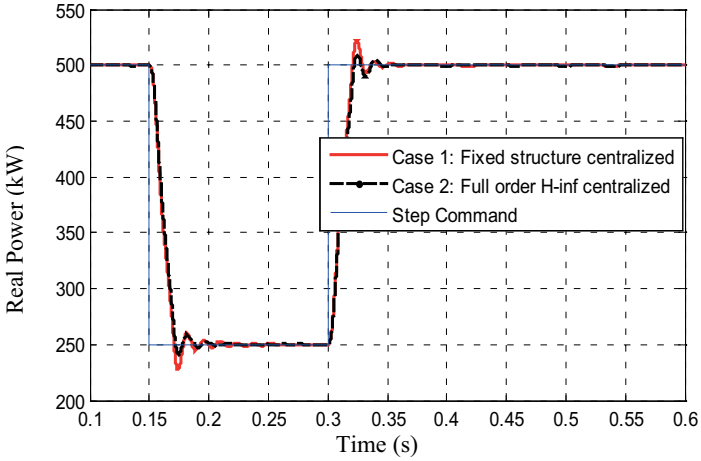

FIGURE 9. Load change with centralized controllers (Case 1: Proposed fixed structure centralized controller, Case 2: Full order H_∞ centralized controller)

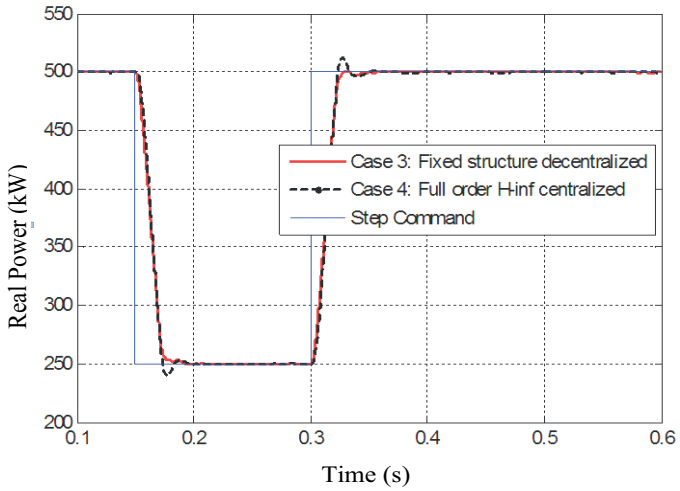

FIGURE 10. Load change with decentralized controllers (Case 3: Proposed fixed structure decentralized controller, Case 4: Full order H_∞ centralized controller)

around the normal values as shown in Table 1. The robustness of the proposed controller is verified by the stability margin in (13) and simulation results illustrated as follows.

Step changes of the DC source voltage: Real power outputs of the three-phase inverter in Cases 1 to 4 from simulations with step changes of the DC source voltage are shown in Figures 7 and 8. The initial DC source voltage v_d is 1,900 V with a reference real power P_{ref} = 500 kW. The DC source voltage is stepped down to 1,800 V at t = 0.15 s, then stepped down again to 1,530 V (70% of normal voltage) at t = 0.3 s.

Step changes of the real power output: With step changes of Load, real power outputs of the three-phase inverter in Cases 1 to 4 from simulations are shown in Figures 9 and 10. The DC source voltage v_d is 1,900 V with a reference real power P_{ref} = 500 kW. The real power of load is stepped down to 250 kW at t = 0.15 s, then stepped up back to 500 kW (50% of rated output power) at t = 0.3 s. As shown in Figures 7-10, all simulations are accomplished in Matlab/Simulink by applying system specifications in Table 1 with simulation time step 2.5 μs. Performance specifications measured from a 0 to 500 kW step command (i.e., rise time, setting time, overshoot and integrated squared error) and stability margin of the controllers in Cases 1 to 4 are shown in Table 2.

Results from all cases depict that all controllers with the three-phase inverter still performs properly under the specific plant uncertainty. Note from Figures 7 to 10 that the proposed controllers in Cases 1 and 3 have a slight difference compared with the full order model in Cases 2 and 4. Although the centralized controllers in Cases 1 and 2 provide higher stability margins, the decentralized controllers in Case 3 offer an advantage on performing lower overshoots during step changes in both DC voltage and load.

5. **Conclusions.** A new technique to design a fixed-structure robust controller for grid connected three-phase inverters is proposed in this paper. Genetic algorithm optimization is applied to determine the optimal controller and weighting function. Performance from the proposed controllers (i.e., centralized and decentralized PID) is compared with conventional H_∞ controller. Although, the conventional H_∞ controllers offer slightly higher stability margin and better overall performance; with significantly lower order controller, implementation of the proposed controllers is considerably less complicated than the conventional H_∞ controller. The proposed technique offers a PID structure controller with

TABLE 2. Performance specifications of the controllers in Cases 1 to 4

Controller	Rise time of real power output (P) (10 to 90%) ms	Setting time of real power output (P) (0 to 2% oscillation)	Percent overshoot of real power output (P)	ISE of output current in direct axis, I_d	Stability Margin
Centralized Fixed Structure Order (Case 1)	0.3	35.1	11.35%	0.0497	0.584
Centralized Full order 1 (Case 2)	0.3	33.6	11.16%	0.0577	0.615
Decentralized Reduced Order (Case 3)	10.0	46.8	6.77%	0.0488	0.546
Centralized Full order 2 (Case 4)	3.5	43.4	4.14%	0.0871	0.627

a guaranteed robust stability margin and desired performance specification. The time domain simulation is accomplished to verify the effectiveness of the proposed controllers.

Acknowledgment. This research work is financially supported by the King Mongkut's Institute of Technology Ladkrabang Research fund and Bangkok University Research Institute.

REFERENCES

[1] F. Blaabjerg, R. Teodorescu, M. Liserre and A. V. Timbus, Overview of control and grid synchronization for distributed power generation systems, *IEEE Trans. Industrial Electronics*, vol.53, no.5, pp.1398-1409, 2006.

[2] M. B. Delghavi and A. Yazdani, A control strategy for islanded operation of a distributed resource (DR) unit, *Proc. of Power & Energy Society General Meeting*, pp.1-8, 2009.

[3] S. M. Muyeen, A. Al-Durra and J. Tamura, Variable speed wind turbine generator system with current controlled voltage source inverter, *Journal of Energy Conversion and Management*, vol.52, no.7, pp.2688-2694, 2011.

[4] N. Nimpitiwan, G. T. Heydt, R. Ayyanar and S. Suryanarayanan, Fault current contribution from synchronous machine and inverter based distributed generators, *IEEE Trans. Power Delivery*, vol.22, no.1, pp.634-641, 2007.

[5] N. Kroutikova, C. A. Hernandez-Aramburo and T. C. Green, State-space model of grid-connected inverters under current control mode, *IET Electr. Power Appl.*, vol.1, no.3, pp.329-338, 2007.

[6] N. Abdel-Rahim and J. E. Quaicoe, Small-signal model and analysis of a multiple feedback control scheme for three-phase voltage-source UPS inverters, *Proc. of Power Electronics Specialists Conference*, Baveno, Italy, vol.1, pp.188-194, 1996.

[7] L. Wang and Y.-H. Lin, Small-signal stability and transient analysis of an autonomous PV system, *Proc. of Transmission and Distribution Conference and Exposition (IEEE/PES)*, pp.1-6, 2008.

[8] F. Katiraei, M. R. Iravani and P. W. Lehn, Small-signal dynamic model of a micro-grid including conventional and electronically interfaced distributed resources, *IET Generation, Transmission & Distribution*, vol.1, no.3, pp.369-378, 2007.

[9] D. McFarlane and K. Glover, A loop shaping design procedure using H_∞ synthesis, *IEEE Trans. Automatic Control*, vol.37, no.6, pp.759-769, 1992.

[10] S. Kaitwanidvilai, Particle swarm optimization based fixed-structure H_∞ loop shaping control of MIMO system, *Proc. of the 27th International Modeling, Identification and Control (IASTED)*, Innsbruck, Austria, 2008.

[11] R. Majumder, B. Chaudhuri, H. El-Zobaidi, B. C. Pal and I. M. Jaimoukha, LMI approach to normalised H_∞ loop-shaping design of power system damping controllers, *Proc. of IEE Generation, Transmission and Distribution*, vol.152, pp.952-960, 2005.

[12] S. Patra, S. Sen and G. Ray, Design of static H_∞ loop shaping controller in four-block framework using LMI approach, *Journal of the International Federation of Automatic Control Automatica*, vol.44, no.8, pp.2214-2220, 2008.

[13] R. Vilanova, P. Balaguer, A. Ibeas and C. Pedret, Expected interaction analysis for decentralized control on TITO systems: Application to IMC based PI/PID controller selection, *International Journal of Innovative Computing, Information and Control*, vol.5, no.10(B), pp.3439-3456, 2009.

[14] P. C. Krause, O. Wasynczuk and S. F. Sudhoff, *Analysis of Electric Machinery and Drive Systems*, 2nd Edition, Piscataway, Wiley Inter Science, New Jersey, 2002.

[15] N. Nimpitiwan and S. Kaitwanidvilai, Robust control design for three-phase power inverters using genetic algorithm, *Proc. of Electrical Engineering/Electronics, Computer, Telecommunications and Information Technology (ECTI-CON)*, Khon kaen, Thailand, pp.756-759, 2011.

Appendix A.

Case 1 Fixed structure centralized controller

$$W_1 = \begin{bmatrix} 0.163 \times 10^{-3} + \frac{0.100}{s} + \frac{0.0102 \times 10^{-6} s}{0.001s+1} & 0 \\ 0 & 0.1335 + \frac{0.2039}{s} + \frac{-0.090 \times 10^{-6} s}{0.001s+1} \end{bmatrix}$$

$$K_{ST} = \begin{bmatrix} 0.8330 & 0.2446 \\ -0.1484 & 0.8156 \end{bmatrix}$$

Case 3 Fixed structure decentralized controller

$$W_1 = \begin{bmatrix} 0.2592 \times 10^{-3} + \frac{0.1747}{s} + \frac{-0.0283 \times 10^{-6} s}{0.001s+1} & 0 \\ 0 & 0.100 + \frac{0.8445}{s} + \frac{-0.3148 \times 10^{-6} s}{0.001s+1} \end{bmatrix}$$

$$K_{ST} = \begin{bmatrix} 0.7783 & 0 \\ 0 & -0.0283 \end{bmatrix}$$